

# Geometrical theory to predict eccentric photorefractive intensity profiles in the human eye

Austin Roorda and Melanie C. W. Campbell

*School of Optometry and Department of Physics, University of Waterloo, and Guelph-Waterloo Program for Graduate Work in Physics, University of Waterloo, Waterloo, Ontario N2L 3G1, Canada*

W. R. Bobier

*School of Optometry, University of Waterloo, Waterloo, Ontario N2L 3G1, Canada*

Received March 30, 1994; revised manuscript received September 6, 1994; accepted October 3, 1994

In eccentric photorefractive, light returning from the retina of the eye is photographed by a camera focused on the eye's pupil. We use a geometrical model of eccentric photorefractive to generate intensity profiles across the pupil image. The intensity profiles for three different monochromatic aberration functions induced in a single eye are predicted and show good agreement with the measured eccentric photorefractive intensity profiles. A directional reflection from the retina is incorporated into the calculation. Intensity profiles for symmetric and asymmetric aberrations are generated and measured. The latter profile shows a dependency on the source position and the meridian. The magnitude of the effect of thresholding on measured pattern extents is predicted. Monochromatic aberrations in human eyes will cause deviations in the eccentric photorefractive measurements from traditional crescents caused by defocus and may cause misdiagnoses of ametropia or anisometropia. Our results suggest that measuring refraction along the vertical meridian is preferred for screening studies with the eccentric photorefractor.

*Key words:* eccentric photorefractive, ocular aberrations, retinal reflections.

## 1. INTRODUCTION

We have set out to develop a simplified geometrical-optical technique for predicting the paths of rays reflected from the retina in nonimaging applications such as eccentric photorefractive. Using this geometrical tool, we analyze the effects of ocular aberrations on the intensity profiles measured across the pupil in photorefractive, the degree and effect of thresholding in traditional measurements, and the effects on and implications of asymmetric aberrations for intensity profiles.

The predicted results from the geometrical model are verified experimentally in a single eye, where differing aberration functions are induced by the application of varifocal contact lenses.

### A. Background

Eccentric photorefractive is a technique for measuring the refractive state of the human eye. The technique is remote from the subject and quick, which makes it particularly useful in refracting the eyes of children or uncooperative subjects for whom traditional methods, such as retinoscopy, are impractical and difficult to perform. The eccentric photorefractor employs a small light source, positioned a fixed distance from the limiting aperture of the camera, that projects a blurred spot onto the retina (Fig. 1). The eccentricity refers to the distance of the light source from the limiting aperture. The camera is focused on the pupil plane, and light reflected from the retina appears as an intensity distribution or crescent in the pupil. The size and the orientation of the crescent are used to determine the refractive state of the eye.<sup>1,2</sup> A set of equations was developed simultaneously

in 1985 by Bobier and Braddick<sup>1</sup> and by Howland,<sup>2</sup> who used a paraxial geometrical theory that gives the refractive state in terms of the crescent width and other measurement parameters such as eccentricity and camera distance. Eccentric photorefractive methods that use an extended light source and measure the slope of the intensity distribution have also been developed.<sup>3</sup>

Our main concern is in the region near the dead zone, where, in the paraxial approximation, no light distribution is expected across the pupil. This dead zone occurs when the eye is focused on the source. One can narrow the width of this dead zone (in refractive state) by reducing the eccentricity of the source. In screening studies the width of this dead zone is set such that ametropias greater than a specified value (say,  $\pm 2$  D) will produce a light distribution. Subjects with ametropias less than this are expected to have no intensity distribution, that is, their refractive states are said to lie in the dead zone. We will show that, in this region, the photorefractor is very sensitive to aberrations. We previously showed that aberrations may cause the misclassification of ametropias and a decrease in instrument sensitivity.<sup>4</sup> For higher refractive states the defocus is the main contributor to the retinal blur, so we show that, as the refractive state increases, the crescent assumes a more traditional form, as is predicted for the aberration-free eye. The important factor in the sensitivity of the eccentric photorefractor to refractive error is the angle subtended between the source and the limiting aperture, which is approximately the eccentricity  $e$  divided by the camera distance from the subject. Therefore our settings of 1-mm eccentricity and 0.33-m working distance used throughout this paper are equivalent to those of an eccentric photorefractor with

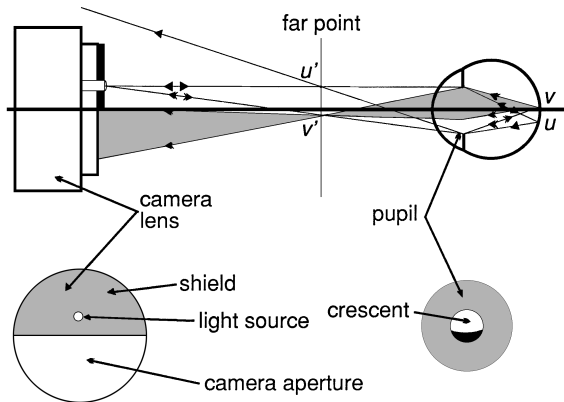


Fig. 1. Light from the source forms a blur  $uv$  on the surface of the retina. The light is diffusely reflected from the retina, and an image of blur  $uv$  can be constructed at the far point of the eye. This aerial image is labeled  $u'v'$ . Some of the rays from point  $v$  pass through  $v'$  and enter the aperture of the camera. These rays are the shaded bundle of rays in the figure. If a ray from a particular point in the pupil enters the camera aperture, then that point on the pupil will appear illuminated. This is how the crescent is formed. The front view of the pupil illustrates the crescent that would appear in this case. In this figure the eye is myopic with no aberrations. One situates the limiting aperture at the source plane by putting a thin shield across one half of the lens. The eccentricity is the distance from the light source to the edge of the shield.

5-mm eccentricity and a 1.67-m working distance (i.e., more-traditional settings).

### B. Effects of Aberrations

The human eye is subject to more than just defocus errors. Chromatic aberrations in the eye are well known and have predictable effects on eccentric photorefractive patterns.<sup>5</sup> The effects of astigmatism on pattern extents and orientations have been explored by Wesemann *et al.*<sup>6</sup> Hodgkinson *et al.*<sup>7</sup> have developed a physical optical model to predict the effects of chromatic, spherical, and astigmatic aberrations on intensity profiles for a knife-edge photorefractor. Their method, however, was based on the assumption that the returned light always tends to a Gaussian form. We show that this is not always the case.

The theory in this paper is based on our previous study that developed a geometrical method to predict the maximum extents of the photorefractive pattern given any general aberration in the eye.<sup>4</sup> This model accounted for the variability of aberrations among eyes and predicted that crescent edge measurements and inferred refractive states can be affected by the presence of aberrations, especially near the dead zone. We showed that the crescent may be larger or smaller than that predicted by paraxial theory, depending on the type of aberration present. We extend this framework to predict the intensity profile given any aberration, and we also verify our predictions experimentally. The new analysis is comparable with that used in the Foucault knife-edge measurement of aberration adopted by Berny and Slansky<sup>8</sup> to measure the wave-front aberration in the eye. Their method, however, eliminated the first pass by illuminating the retina in Maxwellian view. This was technically a more difficult measurement, but it greatly simplified the analysis so that they could measure the wave-front aberration in the pupil from the knife-edge photographic patterns.

Our intention, on the other hand, is to predict the effects of particular aberrations on classical double-pass intensity patterns.

### C. Thresholding

The intensity distribution at the edges of photorefractive patterns is not sharp but decreases gradually. This creates some uncertainty in the measurement of the position of crescent edges and creates a dependency of pattern extent on the particular system (i.e., film sensitivity, camera lens, etc.) and on the person performing the measurement. In general, measured pattern extents are less than that predicted by the theory.<sup>1,2,9</sup> This reduction is not the same for all refractive states, and it was found that in some cases experimental pattern extents may actually exceed theoretical predictions.<sup>1,9</sup> This difference, however, was found by comparisons with the paraxial theory. Monochromatic aberrations have been shown to increase the predicted extents of the patterns.<sup>4,10</sup> Currently, thresholding is dealt with by an experimental calibration for the particular instrument.<sup>9</sup> To our knowledge, no theoretical work has been published that predicts the magnitude of the effect of thresholding on measured refractive states.

### D. Asymmetric Aberrations

We use our geometrical model to calculate the intensity profile along any meridian of the eye. We show that (i) for rotationally symmetric aberrations, such as spherical aberration and defocus, measurements are independent of source position or meridian and (ii) for asymmetric aberrations, such as the complex aberrations found in the human eye,<sup>11</sup> primary astigmatism and coma, the pattern is dependent on the source position and the meridian. The meridian of the source refers to the orientation of the line from the source through the center of the limiting aperture. The position of the source refers to the location of the source with respect to the limiting aperture as viewed by the subject (i.e., nasal, temporal, superior, inferior). We discuss the implications of this dependence for measurements in which two eyes are photorefracted simultaneously. In this analysis we restrict ourselves to measurements along principal astigmatic and comatic meridians.

## 2. GEOMETRICAL-OPTICAL ANALYSIS

A geometrical theory was chosen instead of a physical optical theory to calculate the expected intensity profiles. This approach is justifiable since the aberrations in the human eye are generally greater than one wavelength.<sup>12</sup> Diffraction effects are predominant for aberrations less than one quarter of a wavelength, but, for aberrations that are several times this value, a geometrical approach is reasonable.<sup>13</sup> The geometrical theory has faster calculation times and can take advantage of the existing theory for predicting the location of the crescent edges.

### A. Calculation of the Intensity Profile

The general method followed is one previously developed<sup>4</sup> and is based on similar assumptions. The light source is assumed to be a point. Light from the source enters the eye and is imaged on the retina as a blurred spot. The entering light is traced to the eye ray by ray. Each ray

has an intersection point on the retina determined by the aberration function in the pupil. The aberration function is discussed in terms of transverse [ $t(\mathbf{r})$ ] and longitudinal [ $k(\mathbf{r})$ ] aberrations. The term  $t(\mathbf{r})$  can be defined as the ray intercept position on the retina measured from the paraxial intercept, projected into object space, as a function of the ray's position in the pupil.  $k(\mathbf{r})$  is defined as the far-point distance from the eye as a function of the ray position in the pupil. Both representations define the same aberration according to the relation

$$k(\mathbf{r}) = \frac{l}{\left[1 - \frac{t(\mathbf{r})}{r}\right]}, \quad (1)$$

where  $k(\mathbf{r})$  is the longitudinal aberration (far-point shift),  $t(\mathbf{r})$  is the transverse aberration,  $l$  is the object distance, and  $\mathbf{r}$  is the vector ray position in the pupil. The density of intersecting rays on the retina as a function of ray position defines the retinal point-spread function.

Each point on the retina is assumed to emit light in all directions as a diffuse reflector. The directional component of the reflection is discussed in Subsection 2.B. A principal ray can be drawn from each point on the retinal point-spread function, and it emerges from the center of the entrance pupil. The density of intersecting principal rays in the source plane is a scaled version of the retinal point-spread function (Fig. 2). So the retinal point-spread function is calculated not directly but rather in terms of the principal rays emerging from it. This calculation can be performed without knowledge of any of the optics of the eye other than the aberrations as a function of position in the entrance pupil. The intersection of the principal ray in the source plane is calculated by<sup>4</sup>

$$x_{pr}(\mathbf{r}) = \mathbf{r} \cdot \frac{[p + k(\mathbf{r})]}{-k(\mathbf{r})}, \quad (2)$$

where  $x_{pr}(\mathbf{r})$  is the position of intersection of the principal ray in the source plane with respect to the source (in millimeters),  $\mathbf{r}$  is the ray position in the pupil (millimeters),  $p$  is the camera distance (meters), and  $k(\mathbf{r})$  is the far-point position as function of ray position in the pupil (meters).

We find the density of the projected retinal point-spread function by sampling the intersecting principal rays per unit length in the source plane. The unique feature of the model is that it is suitable for any type of eye, model eye or living eye, provided that the aberration function across the entrance pupil is known.

The diffusely reflected rays emerging from a single point on the retina will intersect their principal ray outside the eye at a far point determined by the radius at which the ray leaves the pupil (Fig. 3). If there are no aberrations present, all rays from a single point on the retina will intersect at a single point along the principal ray. With aberrations present, the intersection point will vary according to the aberration function. In this analysis we assume that the point-spread and the aberration functions are the same in the second pass as in the first.

We determine the maximum crescent extents by tracing the rays from the extreme edge of the blur on the retina and finding which rays enter the limiting aperture of the camera. The original monochromatic theory of the effects of aberrations on photorefraction<sup>4</sup> considered rays

from this point only. Rays from the other points on the retinal blur will not increase the crescent size but will contribute to the crescent intensity. We calculate the crescent intensity profile by first calculating the pattern extents in the pupil for each point on the retinal blur. This is illustrated in Fig. 3 for a general aberration. The edges of the pattern extents for each position on the blur on the retina are given by<sup>4</sup>

$$y(\mathbf{r}) = x_{pr} + \mathbf{r} \cdot \frac{[p + k(\mathbf{r})]}{-k(\mathbf{r})}, \quad (3)$$

where  $y(\mathbf{r})$  is the position of intersection of the returning ray and  $x_{pr}$  is the position of intersection of the principal ray as defined in Eq. (2).

The positions in the pupil,  $\mathbf{r}$ , for which  $y(\mathbf{r}) = e$ , the source eccentricity, are the edges of the crescent from a particular point on the retina.<sup>4</sup> In some cases, such as is shown in Fig. 3, there may be two or more rays from a single point on the retina that intersect the limiting aperture. This is the source of the split patterns (crescents appear to originate from either side of the pupil) and the central bright regions (a pattern in which the peak intensity occurs near the center of the pupil and tails off toward the margins) that often appear in photorefraction profiles.<sup>14</sup>

Each pattern is given an intensity weighting according to the intensity of the corresponding point on the retinal blur, derived from Eq. (2). The sum of all the patterns from each point gives the final intensity profile.

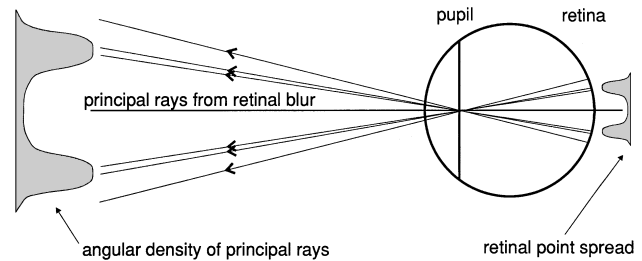


Fig. 2. The principal ray from each point on the retinal blur emerges from the center of the entrance pupil. Thus the angular density of principal rays will be a scaled distribution equivalent to the intensity of the retinal point spread.

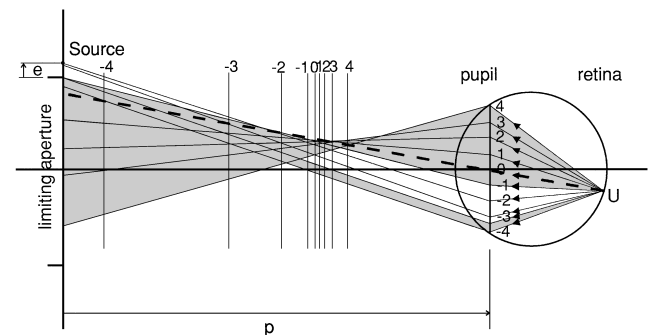


Fig. 3. The diffusely reflected rays from a single point on the retina are traced out of the eye. The principal ray is the heavy dashed line from point U on the retina. This ray trace illustrates several rays traced out of the eye through the points labeled 4 to -4 that intersect the principal ray at the corresponding far points. The bundles of rays (shaded) that enter the limiting aperture of the camera define the regions where crescents will appear in the pupil. In this case a comatic-type aberration combined with defocus results in a split crescent photographed in the pupil plane.

We model the change in the refractive state by adding a constant defocus factor to the aberration function. We assume that the aberrations are constant with object vergence.<sup>4</sup> In this way the crescent intensity profiles can be calculated for a range of refractive errors.

### B. Incorporation of Directional Reflection Effects

The Stiles–Crawford effect of the first kind refers to the perceived intensity of light as a function of the ray entrance position in the pupil. The function peaks near the pupil center and drops off parabolically from this point. Gorrand *et al.*,<sup>15</sup> van Blokland,<sup>16</sup> and Röhler and Schmielau<sup>17</sup> have all found that reflections from the retina have a similar directional feature. This effect is attributed primarily to the limited acceptance angle of a single photoreceptor. The photoreceptor has waveguiding properties like those of a small optical fiber. The intensity of the reflection is generally greatest near the center of the pupil and drops off toward the margins. One can incorporate this reflection effect into the crescent intensity profiles by multiplying the intensity at each point across the pupil by an attenuation factor that is a function of the radius. A function was selected that matched the typical reflection function found by the authors mentioned above<sup>15–17</sup> [Eq. (4) below]. The exponential decay term in the function is similar to that used by Artal,<sup>18</sup> but we have added a baseline term. This function also incorporates a decrease in the directionality with increasing spot size (or increasing refractive state) by means of a change in  $D$ . A calculation of the change in directionality with spot size is included in the results. The form of the attenuation factor chosen was

$$I(r) = I_0 \left\{ \frac{1 + \exp[-D(r/r_{\max})^2]}{2} \right\}, \quad (4)$$

where  $I_0$  is the uncorrected crescent intensity,  $I(r)$  is the attenuated crescent intensity,  $D$  is a directionality factor ( $D = 0 \equiv$  no directionality;  $D = 4 \equiv$  50% attenuation at pupil edges),  $r_{\max}$  is the maximum radius of the pupil (millimeters), and  $r$  is the ray position in the pupil (millimeters).

### C. Calculations

The calculations are iterative and were performed on a computer. The aberration functions were entered into the program as the variation of the far point as a function of the pupil position (longitudinal aberration). A two-dimensional array of the intensity as a function of refractive state and pupil position was generated and plotted as a three-dimensional surface chart.

## 3. EXPERIMENT

An experiment was performed to compare empirical eccentric photorefraction patterns with the theoretical predictions for three ocular aberration functions in the eye. Effects of aberrations, thresholding, and asymmetric aberrations were investigated. We used a single eye to maintain a constancy between the cases, the only difference between them being the aberration of the optical elements. Differences in retinal reflectivity, the direc-

tionality of the retinal reflections, and ocular scatter are ruled out.

The aberrations were induced in the eye by application in two cases of soft varifocal contact lenses of two types, PA1 (Bausch & Lomb, nominal power  $-0.5$  D) and PS45 (Nissel, nominal power  $-0.5$  D), respectively; the third case is for the unaided eye. The lenses were designed with changing power for each annular zone to provide a range of foci to aid vision for the presbyopic eye, which has little or no accommodative facility. The idea is that one could obtain a long depth of focus by inducing spherical aberration with the contact lens in place. Hence the application of these contact lenses is equivalent to inducing monochromatic aberrations in the eye.<sup>19</sup> The lenses have different effects on the aberrations for each person<sup>20</sup> and produce values two to three times larger than that found in an average adult human eye.<sup>11</sup>

The aberrations were measured along the horizontal meridian for three cases: with the PA1 lens, with the PS45 lens, and with the unaided eye, and were used to predict the expected intensity profiles. Measured eccentric photorefraction intensity profiles were then compared with the theoretical predictions. The subject was an emmetrope ( $<0.25$  D) with no astigmatism ( $<0.25$  D), 26 years of age, and without correction had relatively low aberrations across the horizontal meridian. Visual acuity was measured as 20/15.

We measured the aberrations across a single meridian in the eye with and without the contact lenses at a fixed accommodative state, using a previously developed modified Ivanoff apparatus,<sup>11</sup> as the aberrations are known to vary with the accommodative state. The eye was given a stimulus for accommodation at 3 D. In the measurement the observer was required to align a target in a Maxwellian view with a similar target in a normal view. The normal and Maxwellian views were seen simultaneously in a split field. The subject perceives a horizontal separation of the targets that varies with the horizontal position of the Maxwellian view in the pupil. This separation is due to the aberration corresponding to the particular pupil position. By moving the actual position of the target that appears in the Maxwellian view, the subject can achieve a perceived alignment of the two targets. The separation of the targets in real space, after a subjective alignment, for each position of the Maxwellian view across the pupil is directly related to the transverse ray aberration. A fifth-order polynomial is fitted to the transverse aberration to produce a smooth aberration function:

$$t(\mathbf{r}) = A_1 \mathbf{r}^3 + A_2 \mathbf{r}^5 + B_1 \mathbf{r}^2 + B_2 \mathbf{r}^4 + C \mathbf{r} + \Delta t, \quad (5)$$

where  $A_1$  and  $A_2$  are coefficients of third- and fifth-order spherical aberration, respectively,  $B_1$  and  $B_2$  are coefficients of third- and fifth-order coma, respectively,  $C$  is the defocus coefficient, and  $\Delta t$  is the zero-offset term.

The data from the above experiment were converted to longitudinal aberration [Eq. (1)] and input into the computer program for calculating the expected eccentric photorefraction intensity profiles as a function of refractive state; we used the same settings (i.e., working distance, pupil size, and eccentricity) as in the actual measurements (described below). The computer program was

written in BASIC and required less than 1 min on a 486 PC to generate a profile at a single refractive state. For the single profiles, rays were traced through the eye at 0.1-mm intervals across the entrance pupil. For the three dimensional plots rays were traced at 0.3-mm intervals and the refractive state was stepped in 0.3-D intervals. A flow chart of the computer program is included as Appendix A.

An eccentric photorefraction experiment was performed on the same eye fitted in turn with each of the contact lenses and with the unaided eye. The camera distance was 0.33 m to permit high magnification of the pupil. The eccentricity of the source was 1 mm temporal to make the instrument sensitive to small aberrations near zero defocus. We simulated a range of refractive states by placing corrective lenses in front of the eye. The opposite eye fixated on a target at 0.33 m ( $-3$  D accommodative state). We assumed that there was no change in aberrations with vergence, that the additional aberrations induced by the corrective lenses were small compared with those of the eye, and that the accommodative state of the eye was fixed. The light source was limited to a finite bandwidth in the red (620–720 nm). This permitted good reflectivity from the retina and little blurring because of chromatic aberration. The directionality in red light is expected to be less variable because in the bleached or the unbleached state the red-light reflection directionality is virtually unchanged.<sup>16</sup> The images were captured on a CCD array, and the crescent edges and the intensity profiles were measured with an image-analysis software package.

To investigate the thresholding effects we used an unbiased observer to measure the crescent extents, noting traditional patterns and the split and central bright patterns. The measurement technique was simply a subjective measurement of the edges of the photorefraction crescents as would usually be performed. These measured values were compared with the theoretical predictions corrected for different thresholds.

To investigate the effects of asymmetric aberrations, two eccentric photorefraction images were taken with the light source on either side (nasal and temporal) of the horizontal meridian with the PA1 contact lens in place. The images were taken with the opposite eye focused on a light source at 0.33 m.

## 4. RESULTS

A polynomial [Eq. (5)] was fitted to the aberration data for the PA1 lens, the PS45 lens, and no contact lens (Fig. 4). The PA1 induced a positive spherical aberration in the eye with some decentration. The PS45 induced predominantly negative spherical aberration. The aberrations of the eye measured without any lens were quite small, even with respect to a typical human subject.<sup>11</sup>

### A. Intensity Profiles

The experimental results for the eye focused on the source are shown in Fig. 5. For each pupil image the experimental intensity profile is shown, along with the predicted experimental profile. Several steps were made in performing this fit. First, the profile was predicted from the measured aberrations as outlined in Subsection 2.A; then

the directionality factor  $D$  from Eq. (4) was adjusted for a best fit. Fits with no directionality are shown for comparison. The background intensity was assumed to be

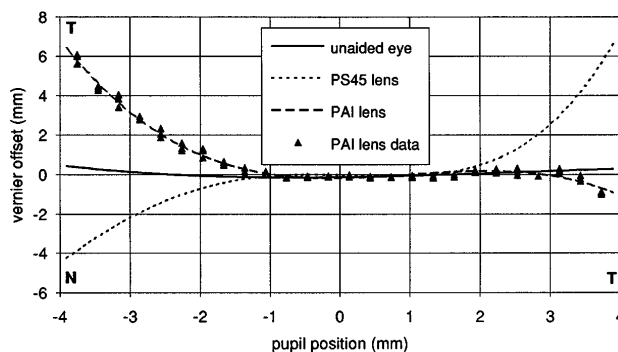


Fig. 4. Transverse aberration data for the three cases measured on a single subject (AR, right eye) at 3 D accommodative state. The data and the curve fit are shown for the PA1 lens to illustrate the accuracy of the fit. The three cases are unaided eye (low aberrations), PA1 lens (asymmetric aberration or decentered positive spherical aberration), and PS45 lens (symmetric, negative spherical aberration).

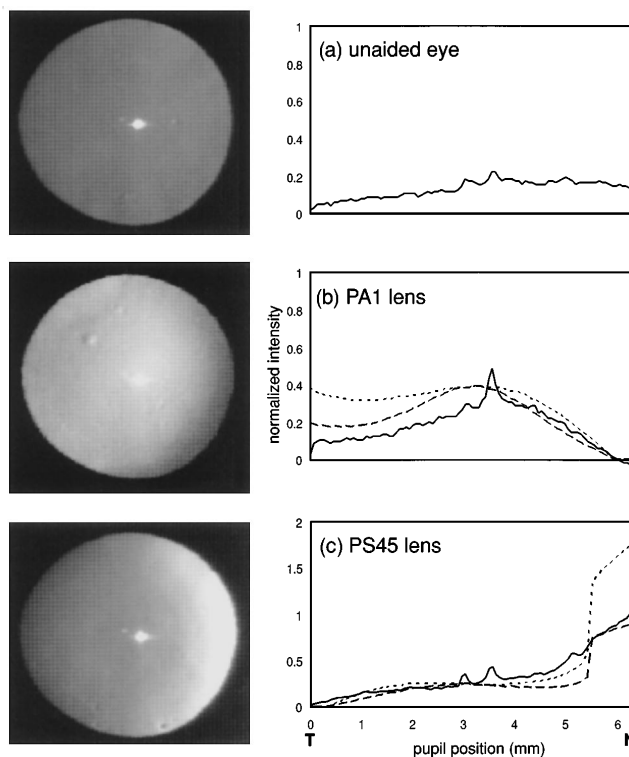


Fig. 5. Eccentric photorefraction images at  $-3$  D paraxial refractive state (focused at the source) obtained by use of a temporal source, 1-mm eccentricity, and a 0.33-m working distance. The images are of the full pupil. The bright spot in the center of the pupil is the first Purkinje image and can be ignored. The experimental profiles (solid curves) are taken directly from the horizontal meridian of the images. The background scatter has been subtracted from each profile. The computer-generated profiles are the expected intensity profiles for the same refractive state. Long-dashed curves are the profiles with directionality, and short-dashed curves represent calculations before directionality was incorporated. (a) Unaided eye: no crescent observed, only background scatter. (b) PA1 lens: diffuse crescent pattern observed extending throughout the pupil with peak intensity close to the center. (c) PS45 lens: crescent with high intensity formed in the nasal margin that drops off rapidly across the pupil. The normalization of the experimental maximum in (c) determines all other intensity levels.

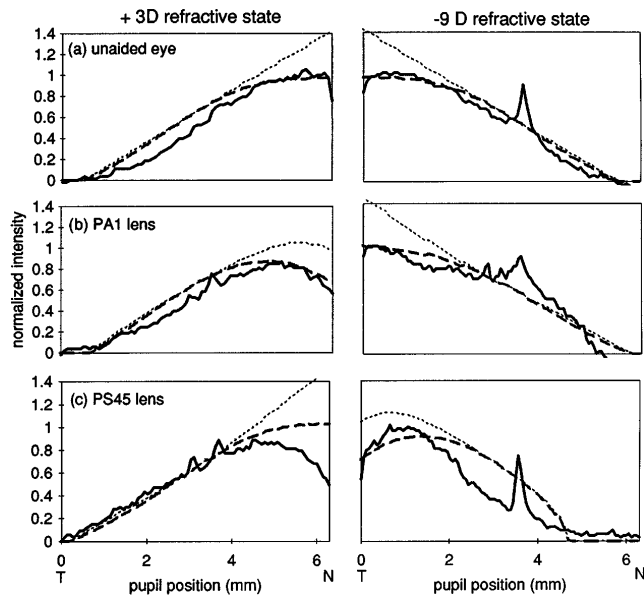


Fig. 6. Experimental versus theoretical predictions for +3 D (left) and -9 D (right) refractive states. These refractive states represent 6 D defocus in either direction from the camera placed 0.33 m from the eye. Solid curves, experimental profiles; long-dashed curves, predicted profiles with directionality; short-dashed curves, predicted profiles without directionality. The plots show that for the three cases the intensity profiles take a similar form. The defocus term is dominant, and the other aberrations have a small effect. (a) Unaided eye, (b) PA1 lens, (c) PS45 lens.

due to scatter and was subtracted for each experimental profile. We did this by subtracting a constant value that was the lowest intensity across the photorefractive intensity profile for the eye with no contact lens at the -3 D nominal refractive state. The same baseline value was subtracted from all three profiles. As the intensity scales for both the theoretical and the experimental profiles were arbitrary, the profiles for both were scaled for a best fit, normalized, and superimposed. The same scaling factors were applied for the three cases. A comparison of the experimental results, measured from Fig. 5, demonstrates the agreement of the predicted results of the geometrical-optical model with the empirical measurements for low refractive states. For the higher refractive states the defocus term dominates, and the crescent takes a more-traditional shape. The same procedure was performed in matching the theoretical with the experimental profiles. A comparison of the experimental and theoretical profiles for refractive errors of 6 D myopic and 6 D hyperopic with respect to the camera position at 0.33 m is shown in Fig. 6. A good fit of the predicted to the experimental profiles was obtained across the entire range of refractive states.

It was found that, as the refractive state increased, the directionality of the retinal reflection for best fit to the data decreased. We calculated the directionality for several of the PA1 and the PS45 results by comparing the theoretical and the experimental profiles and adjusting the factor  $D$  for a best match. The results of the change in directionality as a function of paraxial refractive state are shown in Fig. 7. A directionality factor was not calculated for every condition at each refractive state because the intensity distribution did not always cover enough of

the meridian to provide sufficient data for fitting. The calculated profiles for a range of refractive states for the three cases have been generated incorporating the changing directionality and are shown in Fig. 8.

## B. Thresholding

Traditional crescent-width measurements are often smaller than the theoretical results because the theoreti-

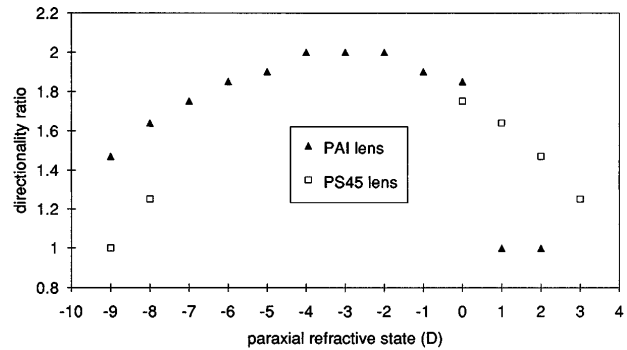


Fig. 7. The directionality of the reflection is determined by the ratio of the intensity at the center of the pupil to the attenuation at the margins [see Eq. (4)]. A higher ratio indicates more directionality. The directionality was deduced from the experimental results and was highest for low refractive errors. The decrease in directionality for high refractive states may indicate some photoreceptor disarray during measurement over large spot sizes on the retina.

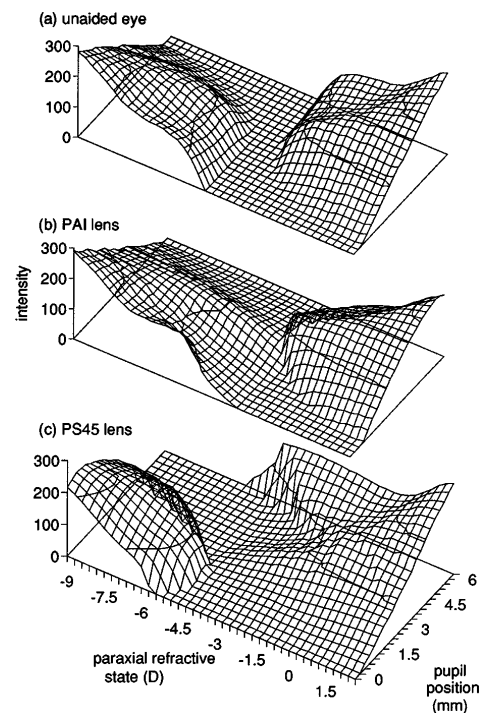


Fig. 8. Computer-generated intensity profiles for a range of refractive states obtained by use of a temporal source, 1-mm eccentricity, and a 0.33-m working distance. The profile for each refractive state has been adjusted for the directionality of the reflection shown in Fig. 9. (a) Unaided eye: with low aberrations, the crescents take a traditional form. There is a dead zone around where the eye is focused on the camera, and crescent intensity increases are symmetric for the hyperopic and myopic regions, except that they originate in opposite margins of the pupil. (b) PA1 lens: the presence of aberration alters the symmetry of the intensity profiles, and the dead zone does not appear. (c) PS45 lens: again the presence of aberration alters the symmetry, and no dead zone occurs.

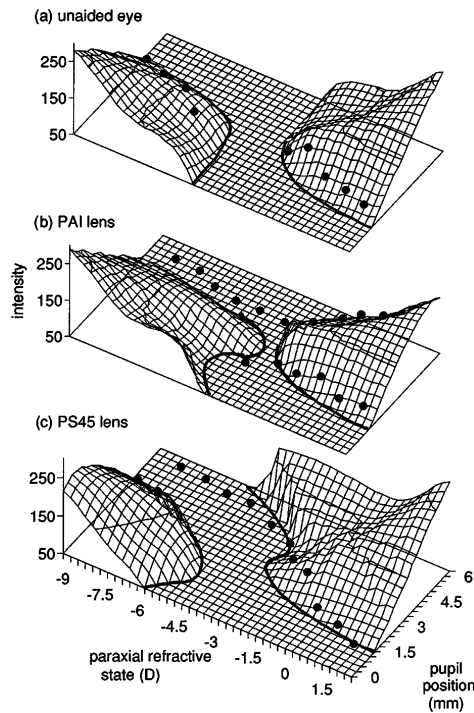


Fig. 9. The baseline has been raised for the three cases. The surface plot represents the theoretical calculations. The predicted edges occur where the surface plots intersect the baseline, given by the solid curves. The points represent empirical measurements of the crescent edges. By raising the baseline, one obtains a good agreement of the experimental measurements with the predicted edges. We obtained the best correction by increasing the baseline by roughly 20% of the maximum intensity as shown.

cal edge does not have sufficient intensity to be measured by the camera. This is a common effect in any photorefractive technique and is referred to as thresholding.<sup>1,2,9,21</sup>

By raising the baseline of any of the intensity profiles shown in Fig. 8, one can obtain a threshold-corrected crescent edge position. An unbiased observer performed crescent-edge measurements for all the experimental results. The measured results originally had poor agreement with the edges predicted by the theory and were less than the prediction in most cases. When the baselines for the three plots in Fig. 8 were raised, a relatively good fit to the measured edges was obtained, indicating that the previous differences had been due to thresholding. We achieved the best agreement by raising the baseline  $\sim 20\%$ . The measured crescent edges are plotted on the threshold-corrected profiles in Fig. 9. Split crescents and central bright regions were observed and are shown in Figs. 9(b) and 9(c).

The threshold correction was also tested on previous data published by Bobier.<sup>9</sup> We raised the baseline of the intensity profiles across the range of refractive states to investigate whether a level could be found that matched the experimental data on a human eye. It was found that a good fit was obtained if the threshold level was raised to 30% of the maximum intensity at the edges. The results are shown in Fig. 10. The degree of thresholding depends on the apparatus used and on the person performing the measurement. A higher-sensitivity system should require a smaller threshold correction. This ac-

counts for the different threshold levels required for Fig. 9 for a video system and Fig. 10 for a photographic system.

### C. Asymmetric Aberrations

The effects of primary coma were investigated as an example of asymmetric aberrations. The theoretical results for a schematic eye with pure primary coma are illustrated in Fig. 11. In this calculation we simulate a source that is on either side (nasal and temporal) of the horizontal meridian.

We used a second PA1 lens in a followup experiment to investigate the effects of asymmetric aberrations on intensity profiles. Figures 12(a) and 12(b) represent the predicted (with directionality) and experimental profiles for the source on the temporal and nasal sides of the horizontal meridian. In both cases the eye was focused on the source. For the aberration-free eye no intensity distribution is expected for either position of the source. If the aberrations were symmetrical the intensity distributions for the temporal and the nasal sources would be symmetrical. Because of the asymmetry of the aberrations induced by the PA1 lens, a considerable difference was observed between the two results.

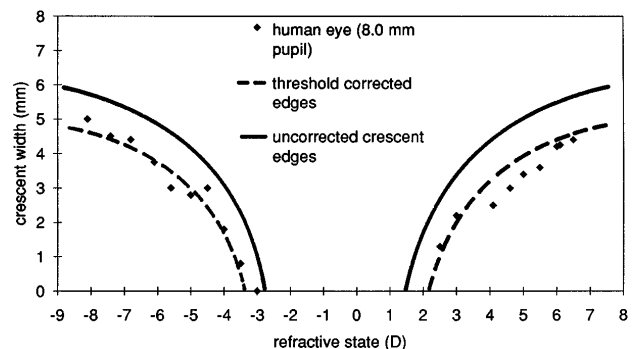


Fig. 10. Threshold-corrected crescent edges for a typical eccentric photorefractive measurement. Camera distance, 1.5 m; eccentricity, 25 mm; pupil size, 8 mm. The solid curves represent the expected crescent edges for a perfect detection system. The dashed curves represent the expected edges if the detection of the edge occurs at 30% of the maximum crescent intensity. The data from a previous study by Bobier<sup>9</sup> (cyclopleged human eye, photographic photorefractive, using 400 ASA color film) fit the threshold-corrected curve.

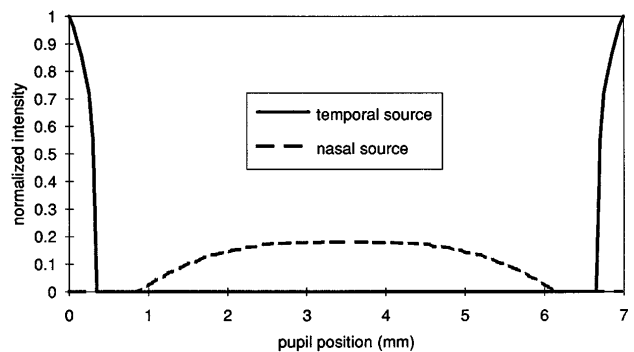


Fig. 11. Dependency of the intensity profiles on the source position for an eye with asymmetric aberrations. In this case the eye is modeled with primary coma along the horizontal meridian. When the source is temporal (solid curve) the result is a split crescent. For the nasal source (dashed curve) a central bright region is observed.

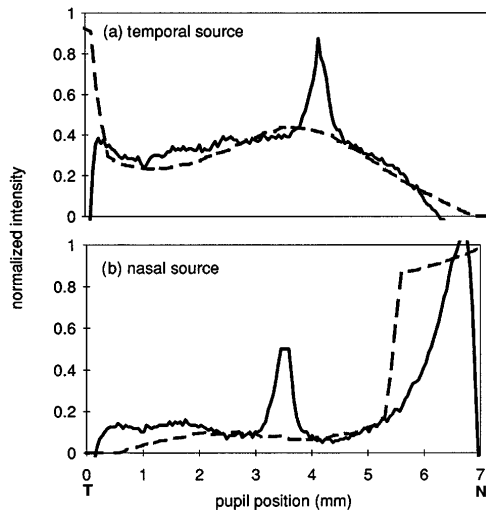


Fig. 12. Two profiles from photorefractive images taken with the PA1 lens with (a) a temporal source and (b) a nasal source. Solid curves, experimental profiles; dashed curves, predicted profiles (with directionality). The peak in the center of the experimental profiles is the Purkinje image and can be ignored. The difference in the two profiles from the nasal and temporal sources indicates the effects of the asymmetric aberration induced by the PA1 lens.

## 5. DISCUSSION

This investigation shows that the geometrical model can be used to predict the general pattern of crescent size and intensity distributions for eccentric photorefractive, given any specific monochromatic aberration distribution in the eye.

Our results verify our expectations that monochromatic aberrations may have considerable effects on photorefractive intensity profiles,<sup>4</sup> especially for low eccentricities and long working distances. Photorefractive pattern extents can be larger or smaller than that predicted by the paraxial theory, but more important, perhaps, is that a wide range of intensity patterns can be seen, especially near the dead zone. Instead of the traditional crescent reflex, one may see split reflexes or central bright spots in the photorefracted pupil. We have shown that these patterns can be explained by the presence of monochromatic aberrations. For aberrations that are rotationally symmetric the pattern will be the same for the source in any meridian. On the other hand, for asymmetric aberrations, such as coma, the photorefracted pattern is highly dependent on the position of the source.

The main effect of aberrations on the intensity profiles occurs for paraxial refractive states when the eye is focused near the source position. In the paraxial model a dead zone occurred for low refractive states for which no intensity distribution appeared in the pupil. Thus, when intensity patterns are observed in this range, they can be attributed to the aberrations alone. Conversely, in a clinical situation, patterns that appear because of aberrations may be mistaken as being due to refractive errors. As the refractive state increases, defocus becomes dominant, and the photorefractive profiles take a more typical form.

Some differences are expected to occur between theoretical and experimental results for several reasons. Ac-

commodative lag for the 3 D stimulus will cause some uncertainty of the precise paraxial refractive state for each measurement. The extended source, multiple layer reflections<sup>22</sup> from the retina, and additional widening of the blur on the retina resulting from light scattered at the fundus<sup>23</sup> will all tend to smooth out the intensity profiles across the pupil. These effects are particularly visible in the disparity between experimental and theoretical results in Fig. 6(c), where the experimental profile appears smoother than predicted. These effects, in general, do not appear large, given the good agreement between theory and experiment, which indicates that the light in the retina scatters at such wide angles that it can be simply modeled as a diffuse reflection from a single layer. A wide-angled broadening of a point source of light may occur as a result of multiple scatter in the fundus,<sup>24</sup> and this reflection could be modeled as a very wide Gaussian base added to, but not convolved with, the retinal point spread. This wide-angle scatter could be used to predict the constant background observed in our measurements.

We expect that the aberrations in the eye are similar for the left and right eyes of the human with respect to the nasal, temporal, superior, and inferior positions.<sup>11</sup> In an application of eccentric photorefractive in which two eyes are measured simultaneously with the source in the horizontal meridian, the source will be nasal for one eye and temporal for the other. On the other hand, if the source is vertical, then the source symmetry will be the same for both eyes, either superior or inferior. Therefore, if the aberrations present are asymmetric and the same for both eyes, the measured photorefractive patterns in both eyes will differ for a horizontal source and will be similar for a vertical source when the eyes are measured simultaneously. A measured difference when the horizontal source is used might be misdiagnosed as anisometropia when, in fact, it is due only to asymmetry of the measurement.

Over the past decade screening of children's refractive errors has been conducted by photographic studies<sup>25-32</sup> such as the Brückner test, based on the principle of eccentric photorefractive. In these studies the child is usually focused on the camera, where the effects of the aberrations are greatest. Little is known about the degree of monochromatic aberrations present in children's eyes, so one should not ignore the fact that high aberrations may exist. Most of these techniques measure both eyes simultaneously in the horizontal meridian. Caution must be taken, then, to ensure that such an instrument does not just detect an asymmetric aberration in the eyes.

To avoid these problems one should subtend a larger angle between the source and the aperture (by increasing eccentricity or decreasing the working distance). This, of course, will increase the minimum refractive state that can be detected by the instrument and decrease the test's sensitivity. One should also ensure that simultaneous measurements of two eyes be made along the vertical direction on the assumption that the aberrations are the same in both eyes.

It should be noted that aberrations in the eye, while they are important in instrumentation, such as photorefractive and ophthalmoscopy, have not been shown to be severely debilitating to the function of the eye. Aberrations are generally greatest at the edges of a

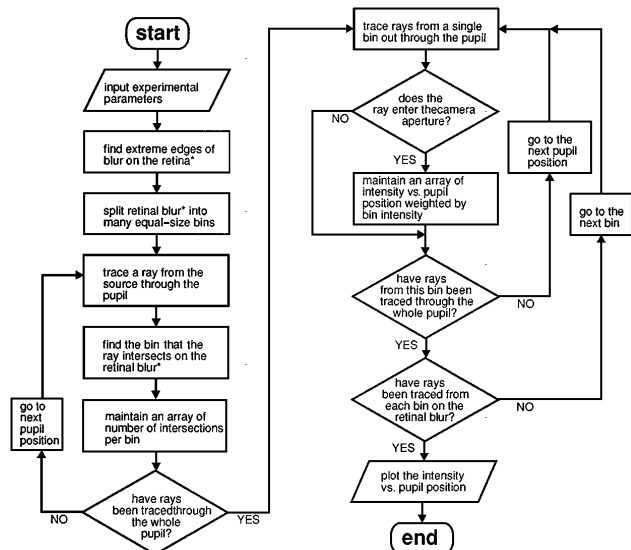
large pupil, where the eye tends to compensate for the blur through the Stiles–Crawford effect or a smaller pupil size.

As the refractive state increased, the directionality needed for prediction of the experimental results decreased (Fig. 7). Thus the directionality of the retinal reflections decreases with increasing spot size on the retina. As the existence of directionality is due to photoreceptor optics, the loss in directionality is probably due to photoreceptor disarray over larger areas on the retina. Some differences between the directionality with the PA1 and PS45 lenses can be seen in Fig. 7. These differences could not be explained by differences in the spot size resulting from the specific aberrations induced by the contact lenses. Therefore the differences are probably due to some variability in the experimental results. In general, however, the trend of decreasing directionality with increasing retinal spot size is found.

The degree of thresholding is dependent on the shape of the intensity profile. If we assume that an edge will be detected at a specific intensity, then one can make the prediction of the threshold-corrected crescent edges by simply increasing the baseline of the intensity plots. The detection of an edge could also be attributed to the rate of change of intensity of the profile, but this effect has not been investigated.

With increasing computational speeds, these iterative geometrical modeling techniques can be used to generate reasonably accurate predictions of intensity distributions for a number of different situations. The model is flexible enough that calculations can be made for many different configurations of the eccentric photorefractor and the influences of monochromatic aberrations in these situations, including extended sources, small camera apertures (retinoscopy simulations), and multiple layers contributing to reflections from the retina. We are exploring these applications at present.

## APPENDIX A: FLOW CHART FOR COMPUTER MODELING OF PHOTOREFRACTION



\*This is the retinal blur projected into object space.

## ACKNOWLEDGMENTS

Thanks to Shannon Cerniuk, Linda Voisin, Peiliang Zheng, and Chengwan Lu for their assistance in the experiments. Support from Hughes Leitz Optical Technologies and the Natural Sciences and Engineering Research Council (NSERC) Canada, is gratefully acknowledged.

## REFERENCES

- W. R. Bobier and O. J. Braddick, "Eccentric photorefraction: optical analysis and empirical measures," *Am. J. Optom. Physiol. Opt.* **62**, 614–620 (1985).
- H. C. Howland, "Optics of photoretinoscopy: results from ray tracing," *Am. J. Optom. Physiol. Opt.* **62**, 621–625 (1985).
- F. Schaeffel, H. C. Howland, S. Weiss, and E. Zrenner, "Measurement of the dynamics of accommodation by automated real time photorefraction," *Invest. Ophthalmol. Vis. Sci.* **34**, 1306 (1993).
- M. C. W. Campbell, W. R. Bobier, and A. Roorda, "Effect of monochromatic aberrations on photorefraction," *J. Opt. Soc. Am. A* **12**, 1637–1646 (1995).
- A. Roorda, W. R. Bobier, and M. C. W. Campbell, "The effect of the eye's chromatic aberration on eccentric photorefraction," in *Ophthalmic and Visual Optics and Noninvasive Assessment of the Visual System*, Vol. 3 of 1993 OSA Technical Digest Series (Optical Society of America, Washington, D.C., 1993), pp. 146–149.
- W. Wesemann, A. M. Norcia, and D. Allen, "Theory of eccentric photorefraction (photoretinoscopy): astigmatic eyes," *J. Opt. Soc. Am. A* **8**, 2038–2047 (1991).
- I. J. Hodgkinson, K. M. Chong, and A. C. B. Moltano, "Photorefraction of the living eye: a model for linear knife edge photoscreening," *Appl. Opt.* **30**, 2263–2269 (1991).
- F. Berny and S. Slansky, "Wavefront determination resulting from Foucault test applied to the human eye and visual instruments," in *Optical Instruments and Techniques*, J. D. Home, ed. (Oriel, London, 1969), pp. 375–385.
- W. R. Bobier, "Eccentric photorefraction: a method to measure accommodation of highly hypermetropic infants," *Clin. Vision Sci.* **5**, 45–66 (1990).
- N. Sayles and H. C. Howland, "Relation of the retinoscopic reflex to the monochromatic aberration of the eye," *Invest. Ophthalmol. Vis. Sci. Suppl.* **26**, 142 (1985).
- M. C. W. Campbell, E. M. Harrison, and P. Simonet, "Psychophysical measurement of the blur on the retina due to optical aberrations of the eye," *Vision Res.* **30**, 1587–1602 (1990).
- W. N. Charman, "Optics of the human eye," in *Vision and Visual Dysfunction*, J. Cronly-Dillon, ed. (CRC, Boca Raton, Fla., 1991), Vol. 1, W. N. Charman, ed., pp. 1–14.
- W. J. Smith, *Modern Optical Engineering*, 2nd ed. (McGraw-Hill, New York, 1990).
- W. R. Bobier, "Eccentric photorefraction," Ph.D. dissertation (University of Cambridge, Cambridge, 1987).
- J.-M. Gorrard, A. Alfieri, and J.-Y. Boire, "Diffusion of the retinal layers of the living human eye," *Vision Res.* **24**, 1097–1106 (1984).
- G. J. van Blokland, "Directionality and alignment of the foveal receptors, assessed with light scattered from the human fundus *in vivo*," *Vision Res.* **26**, 495–500 (1986).
- R. Röhler and F. Schmeilau, "Properties of isolated frog retinæ in reflecting non-polarized and polarized light," *Vision Res.* **16**, 241–246 (1976).
- P. Artal, "Incorporation of directional effects of the retina into computations of optical transfer function of human eyes," *J. Opt. Soc. Am. A* **6**, 1941–1944 (1989).
- W. N. Charman and B. Saunders, "Theoretical and practical factors influencing the optical performance of contact lenses for the presbyope," *J. Brit. Cont. Lens Assoc.* **13**, 67–75 (1990).
- M. C. W. Campbell, W. N. Charman, L. Voisin, and C. Cui, "Psychophysical measurement of the optical quality of vari-

- focal contact lenses," in *Ophthalmic and Visual Optics and Noninvasive Assessment of the Visual System*, Vol. 3 of 1993 OSA Technical Digest Series (Optical Society of America, Washington, D.C., 1993), pp. 12–15.
21. H. C. Howland, O. J. Braddick, J. Atkinson, and B. Howland, "Optics of photorefraction: orthogonal and isotropic methods," *J. Opt. Soc. Am.* **73**, 1701–1708 (1983).
  22. F. C. Delori and K. P. Pflibsen, "Spectral reflectance of the human ocular fundus," *Appl. Opt.* **28**, 1061–1077 (1989).
  23. I. J. Hodgkinson, P. B. Greer, and A. C. B. Molteno, "Point spread function for light scattered in the human ocular fundus," *J. Opt. Soc. Am. A* **11**, 479–486 (1994).
  24. W. N. Charman, "Reflection of plane-polarized light by the retina," *Br. J. Physiol. Opt.* **34**, 34–49 (1980).
  25. K. Kaakinen, H. O. Kaseva, and K. Eeva-Raija, "Mass screening of children for strabismus or ametropia with two flash photostiascopy," *Acta Ophthalmol.* **64**, 105–110 (1986).
  26. K. Kaakinen and L. Ranta-Kemppainen, "Screening of infants for strabismus and refractive errors with two-flash photorefraction with and without cycloplegia," *Acta Ophthalmol.* **64**, 578–582 (1986).
  27. D. P. Crewther, P. M. Kiely, A. McCarthy, and S. G. Crewther, "Evaluation of paraxial photorefraction in screening a population of monkeys for refractive errors," *Clin. Vision Sci.* **3**, 213–220 (1988).
  28. R. H. Duckman and B. Meyer, "The use of photoretinoscopy as a screening technique in the assessment of anisometropia and significant refractive error in infants/toddlers/children and special populations," *Am. J. Optom. Physiol. Opt.* **64**, 604–610 (1987).
  29. C. Hsu-Winges, R. D. Hamer, A. M. Norcia, H. Wesemann, and C. Chan, "Polaroid photorefractive screening of infants," *J. Pediatr. Ophthalmol. Strabismus* **26**, 254–260 (1989).
  30. R. A. Kennedy and S. B. Sheps, "A comparison of photo-screening techniques for amblyopic factors in children," *Can. J. Ophthalmol.* **24**, 259–264 (1989).
  31. A. C. B. Molteno, I. Hoare-Nairne, I. C. Parr, A. Simpson, I. J. Hodgkinson, N. E. O'Brien, and S. D. Watts, "The Otago photoscreener, a method for the mass screening of infants to detect squint and refractive errors," *Trans. Ophthalmol. Soc. N. Z.* **35**, 43–49 (1983).
  32. J. Sjostrand, M. Abrahamsson, G. Fabain, and O. Weinhall, "Photorefraction: a useful tool to detect refraction errors," *Acta Ophthalmol. Suppl.* **157**, 46–52 (1983).